Journal of the American College of Cardiology
© 2012 by the American College of Cardiology Foundation
Published by Elsevier Inc.

Vol. 59, No. 8, 2012
ISSN 0735-1097/$36.00
doi:10.1016/j.jacc.2011.10.888

Catheter-Deliverable Hydrogel Derived From Decellularized Ventricular Extracellular Matrix Increases Endogenous Cardiomyocytes and Preserves Cardiac Function Post-Myocardial Infarction

Jennifer M. Singelyn, PhD,* Priya Sundaramurthy, MS,* Todd D. Johnson, BS,* Pamela J. Schup-Magoffin, BA,* Diane P. Hu, MS,* Denver M. Faulk, BS,* Jean Wang, BS,* Kristine M. Mayle, BS,* Kendra Bartels, RN,† Michael Salvatore, BS,‡ Adam M. Kinsey, PhD,‡ Anthony N. DeMaria, MD,† Nabil Dib, MD, MSc,† Karen L. Christman, PhD*

La Jolla and San Diego, California

Objectives This study evaluated the use of an injectable hydrogel derived from ventricular extracellular matrix (ECM) for treating myocardial infarction (MI) and its ability to be delivered percutaneously.

Background Injectable materials offer promising alternatives to treat MI. Although most of the examined materials have shown preserved or improved cardiac function in small animal models, none have been specifically designed for the heart, and few have translated to catheter delivery in large animal models.

Methods We have developed a myocardial-specific hydrogel, derived from decellularized ventricular ECM, which self-assembles when injected in vivo. Female Sprague-Dawley rats underwent ischemia reperfusion followed by injection of the hydrogel or saline 2 weeks later. The implantation response was assessed via histology and immunohistochemistry, and the potential for arrhythmogenesis was examined using programmed electrical stimulation 1 week post-injection. Cardiac function was analyzed with magnetic resonance imaging 1 week pre-injection and 4 weeks post-MI. In a porcine model, we delivered the hydrogel using the NOGA-guided MyoStar catheter (Biologics Delivery Systems, Irwindale, California), and utilized histology to assess retention of the material.

Results We demonstrate that injection of the material in the rat MI model increases endogenous cardiomyocytes in the infarct area and maintains cardiac function without inducing arrhythmias. Furthermore, we demonstrate feasibility of transendocardial catheter injection in a porcine model.

Conclusions To our knowledge, this is the first in situ gelling material to be delivered via transendocardial injection in a large animal model, a critical step towards the translation of injectable materials for treating MI in humans. Our results warrant further study of this material in a large animal model of MI and suggest this may be a promising new therapy for treating MI. (J Am Coll Cardiol 2012;59:751–63) © 2012 by the American College of Cardiology Foundation

Cardiovascular disease continues to be the leading cause of death in the United States, as well as the rest of the western world, with an estimated 785,000 new myocardial infarctions (MIs) each year (1). Post-MI pathological changes are often progressive, consisting of an initial inflammatory phase, followed by the up-regulation of matrix metalloproteinases that degrade the extracellular matrix (ECM), leading to infarct expansion and wall thinning, and eventual collagen scar deposition to resist deformation and rupture. The resultant negative left ventricular (LV) remodeling is thought to independently contribute to progressive deterioration of cardiac function leading to heart failure post-MI (2). When end-stage failure occurs, heart transplantation or implantation of an LV assist device are the only available treatments. Therefore, the development of new therapies is necessary.

One of the first alternatives to heart transplantation was a technique termed cellular cardiomyoplasty. This technique con-

From the *Department of Bioengineering, University of California, San Diego, La Jolla, California; †School of Medicine, University of California, San Diego, San Diego, California; and ‡Ventrix, Inc., San Diego, California. This research was supported in part by the National Institutes of Health (NIH) Director's New Innovator Award Program, part of the NIH Roadmap for Medical Research, through grant number 1-DP2-OD004309, the Wallace H. Coulter Foundation (Miami, Florida), and National Science Foundation grant NSF 1014429. Mr. Salvatore and Dr. Kinsey are employees of Ventrix, Inc. Dr. DeMaria is on the scientific advisory board of Ventrix, Inc. Dr. Dib is a consultant for Biologics Delivery System. Drs. Dib and Christman hold equity interest in Ventrix, Inc. All other authors have reported that they have no relationships relevant to the contents of this paper to disclose. Joshua M. Hare, MD, FACC, FAHA, served as Guest Editor of this paper.

Manuscript received August 25, 2011; revised manuscript received October 27, 2011, accepted October 28, 2011.

Abbreviations and Acronyms

ECG = electrocardiogram

ECM = extracellular matrix

ED = end-diastole

EDV = end-diastolic volume

EF = ejection fraction

ES = end-systole

ESV = end-systolic volume

H&E = hematoxylin and eosin

IHC = immunohistochemistry

LC-MS/MS = liquid chromatography mass spectrometry

LV = left ventricle

MI = myocardial infarction

MRI = magnetic resonance imaging

SDS = sodium dodecyl sulfate

VT = ventricular tachycardia

sists of injecting cells, suspended in saline or cell culture medium, into the recipient's myocardium (3–9). This is an attractive approach because it allows for minimally invasive intramyocardial delivery through a catheter. Although many clinical trials using cellular cardiomyoplasty have shown some promise (3,6–9), cell retention, engraftment, and survival have been difficult to achieve, due in part to the lack of an appropriate extracellular microenvironment (10). Thus, approaches using cardiac tissue engineering have begun utilizing synthetic and natural biomaterials as scaffolds to improve transplanted cell survival (11), or as stand-alone acellular scaffolds to replace the degraded cardiac ECM, preserve or improve cardiac function, and attenuate LV remodeling (12–15). Injectable biomaterials are particularly attractive since they have the potential to be delivered using a minimally invasive approach, and a material-only therapy would eliminate many of the complications associated with cell therapies.

We have developed a myocardial matrix hydrogel, derived from decellularized ventricular porcine ECM, which is the first cardiac-specific injectable material, offering a replacement scaffold that mimics the native cardiac extracellular environment (16). The myocardium was first decellularized using a perfusion-based technique to generate an intact 3-dimensional scaffold (17). In contrast, we process the ventricular ECM into an injectable liquid that self-assembles upon injection in vivo to form a nanofibrous and porous scaffold. This material offers a biochemical and structural composition that mimics the native ventricular ECM. Herein, we tested the safety and efficacy of injecting the myocardial matrix hydrogel in a rat myocardial infarction model. We demonstrate that injection of myocardial matrix increases endogenous cardiomyocytes in the infarct area and preserves cardiac function post-MI, without increasing incidences of arrhythmia. Considering that many biomaterials being explored as cardiac therapies in small animal models do not have the appropriate properties to translate to catheter delivery in the heart (18), we also tested the ability of the myocardial matrix hydrogel to be delivered via catheter in a porcine model. We demonstrate that the myocardial matrix can be delivered to the myocardium via a percutaneous transendocardial approach, thus paving the way towards clinical translation of a new minimally invasive, biomaterial-based therapy for MI.

Methods

Myocardial matrix preparation. The myocardial matrix was decellularized and prepared as previously described (16). Briefly, Yorkshire farm pigs (35 to 45 kg) were euthanized using an overdose of pentobarbital (90 mg/kg) administered intravenously, and their hearts were then removed. The ventricular tissue was isolated and cut into small rectangular pieces, rinsed in phosphate-buffered saline, and decellularized using 1% sodium dodecyl sulfate (SDS), until the ECM was white. Following completed decellularization, prior to lyophilization, aliquots of the decellularized ECM was then rinsed with deionized water overnight, lyophilized, and milled into a fine powder. Following complete decellularization, prior to lyophilization, aliquots of decellularized ECM were fresh frozen in Tissue-Tek OCT compound (Sakura Finetek, Torrence, California), sectioned into 5 μm slices, and stained with hematoxylin and eosin (H&E) stain to confirm decellularization. The ECM powder was solubilized by enzymatic digestion using pepsin and 0.1 mol/l HCl for at least 54 h prior to use, as modified from a previously published protocol (19). The liquid myocardial matrix was adjusted to pH 7.4 with NaOH, on ice, and brought to 6 mg/ml for injection. A Blyscan sulfated glycosaminoglycan assay (Biocolor, Carrickfergus, United Kingdom) was used to confirm sulfated glycosaminoglycan content (16). For catheter compatibility tests in the porcine model and for identification at 1 week post-injection in the rat model, the material was biotin labeled. For biotin labeling, a 10 mmol/l solution of EZ link Sulfo-NHS-Biotin (Pierce, Rockford, Illinois) was prepared and mixed with the liquid myocardial matrix for a final concentration of 0.3 mg biotin/1 mg matrix. The mixture was allowed to sit on ice for 2 h prior to use.

Liquid chromatography mass spectrometry. Liquid chromatography mass spectrometry (LC-MS/MS) was used to analyze the myocardial matrix, to ensure retained protein content. Lyophilized powder samples were digested in trypsin, in preparation for LC-MS/MS. Electrospray ionization experiments were run on a QSTAR-Elite hybrid mass spectrometer (AB/MDS Sciex, Foster City, California) interfaced to a reversed-phase high-pressure liquid chromatograph. The column used was a 10 cm − 180 ID glass capillary packed with 5-μm C18 Zorbax beads (Agilent Technologies, Santa Clara, California). Peptides were eluted from the C18 column into the mass spectrometer using a linear gradient of 5% to 80% Buffer B (100% acetonitrile, 0.2% formic acid, and 0.005% trifluoroacetic acid) over 60 min at 400 μl/min. (Buffer A was composed of 98% H_2O, 2% acetonitrile, 0.2% formic acid, and 0.005% trifluoroacetic acid). LC-MS/MS data were acquired in a data-dependent fashion, time-of-flight MS were acquired at m/z 400 to 1,600 Da, and MS/MS data were acquired from m/z 50 to 2,000 Da. Once collected, peptide identifications were based on at least 1 peptide with the confidence of above 99% for that peptide identification, using Protein Pilot 2.0 (Life Technologies, Carlsbad, California).

Rat MI and injection surgical procedures. All experiments in this study were performed in accordance with the guidelines established by the Committee on Animal Research at the University of California, San Diego, and the American Association for Accreditation of Laboratory Animal Care. Animal numbers used in each experimental subset are reported in Table 1. MI was induced via 25-min ischemia-reperfusion surgery on female Sprague Dawley rats (225 to 250 g). Animals were anesthetized with 5% isoflurane, intubated, and maintained at 2.5% isoflurane. A left thoracotomy (20) was performed to allow access to the heart, the pericardial sac removed, and a single 6-0 silk suture was placed into the myocardium, around the left coronary artery. The 6-0 suture was tied in a loop, knotted at the end of the loop, a 3-0 silk suture was tied over the knot, and then the 3-0 suture was pulled through the 6-inch PE90 tubing to occlude the artery for 25 min. Ischemia-reperfusion for as little as 17 min with this method of occlusion has been shown to cause consistent infarcts (21,22). After 25 min, the tubing was released, and the suture was removed, allowing the vessel to reperfuse. The animal was then sutured and allowed to recover. Two weeks post-MI, rats were randomized to ensure a similar distribution of ejection fraction (EF) in each group based on baseline magnetic resonance imaging (MRI) measurements, and injected with 75 μl of either saline or solubilized myocardial matrix at 6 mg/ml following a procedure previously described (13,16,22). Briefly, an incision was made in the abdomen, and the diaphragm was cut to expose the heart. A single injection of material was delivered through a 30-gauge needle into the LV wall, and was confirmed by a lightening of the tissue. After injection, the abdomen was stitched closed after suction of the chest cavity, and animals were allowed to recover. For both surgical procedures, animals were given 0.05 mg/kg of buprenorphine hydrochloride (Reckitt Benckiser Healthcare [UK], Hull, United Kingdom), an analgesic, prior to recovery from anesthesia. Animals were also given 3 ml of lactated Ringers (Hospira, Lake Forest, Illinois) solution for hydration during surgery.

Programmed electrical stimulation. To test arrhythmia inducibility, programmed electrical stimulation was performed on hearts, 1 week post-injection. Rats were anesthetized, as previously described, and surgical access to the heart was gained. A pacing electrode was inserted gently into the viable region of the LV wall, such that the exposed electrode tip came in contact with the interior of the LV wall, and the necessary voltage was determined, using a fixed rate pacing (pulse width of 1 ms, cycle length of 120 ms), which was increased until pacing was induced, and voltage was then doubled for the rest of the pacing protocol. The electrocardiogram (ECG) was recorded throughout the pacing procedure, using an ECG signal recorder (DATAQ di-148, DATAQ Instruments, Akron, Ohio), for 1 full hour. Burst pacing and extra-stimulus testing were induced, according to methods previously developed (23–25). After each pacing test, the ECG was observed for any induced arrhythmias; incidences of ventricular tachycardia (VT) were recorded. At the end of the entire burst pacing and extra-stimulus pacing procedures for the rat, the ECG recording was stopped and saved. The heart was excised and fresh frozen for histological analysis.

Table 1 Animal Numbers

	Saline	Matrix
Arrhythmia inducibility, rat	16	20
Histology and IHC, rat	5	5
Functional assessment, rat	6	6
Catheter delivery, pig		2

IHC = immunohistochemistry.

Magnetic resonance imaging. Cine-MRI was performed on a 7-T Bruker magnet, at the UC San Diego fMRI center, using an ECG-triggered fast low-angle shot (FLASH) gradient echo pulse sequence. The following parameters were used: flip angle = 15°, echo time = 1.28 ms, repetition time = 7.7 ms, data matrix = 256 $\times$ 128, field of view = 50 mm^2, slice thickness = 1 mm, and 25 phases were collected per cardiac cycle. Scanning parameters and methods were modified from those determined effective to evaluate ventricular geometry in murine models (26–28). Briefly, rats were anesthetized with isoflurane, while monitoring heart rate and respiratory rate. The long axis of the heart was identified, and subsequent contiguous short-axis slices were acquired throughout the cardiac cycle from apex of the heart to the base of the heart. Images were acquired using a gating system, so that the first image corresponds to end-diastole (ED). Image J (NIH, Bethesda, Maryland) was used to manually outline the endocardial surface for each slice corresponding to ED and end-systole (ES), for the calculation of ventricular area. Although true ES occurs upon opening of the mitral valve and can be detected in echocardiography images (29), for consistency of image analysis, ES is identified as minimal LV lumen area. Each area was then multiplied by slice thickness (1 mm) to calculate LV volume. End-diastolic volume (EDV) and end-systolic volume (ESV) were calculated, allowing for the calculation of EF. From the volume obtained at ED and ES, EF (%) was calculated to be: $([EDV - ESV]/EDV) \times 100\%$. At 1-week post-MI, MR images were taken for evaluation of baseline pre-injection parameters. At 6 weeks post-MI (4 weeks post-injection), hearts were again assessed as described in earlier text. EF and LV geometry were compared pre- and post-injection therapy, thus allowing each animal to serve as its own internal control. Healthy animals were also imaged, revealing an EF of 74 $\pm$ 5% for our model. Rats that did not present an EF representative of an infarct (<69%, 1 standard deviation from a healthy animal) at 1 week were eliminated from the study.

Catheter delivery in a porcine model. Biotin-labeled myocardial matrix was tested for clinical feasibility within a porcine model using a MyoStar Intramyocardial Injection device for transendocardial delivery, as developed for minimally invasive cellular transplantation (4,5). Two Yucatan mini pigs (28 to 40 kg) were used for the study. For 1 animal, pre-anesthesia, Telazol (5 mg/kg, tiletamine HCl and zolazepam HCl, Fort Dodge Animal Health, Fort Dodge, Iowa) was administered, followed by the anesthetic propofol (2.4 mg/kg), until effect, and atrophine (0.02 mg/kg). The animal was intubated, and ventilated with 1% to 2.5% isoflurane and 1 l/min oxygen. An 8-F arterial sheath was inserted through the right femoral artery for access to the LV. Coronary angiography was performed for visualization of the arteries, and the ECG was monitored throughout the surgery. Myocardial matrix was biotin labeled prior to injection for histological post-operative identification, and kept on ice until time of injection. Prior to injection, a unipolar electromechanical map (NOGA) was created of the endocardial wall and used to guide injection. The injection, through a 27-gauge retractable needle, followed protocols commonly used for cellular delivery (4,5,9). Here, a 1-ml Luer lock syringe was loaded with myocardial matrix and attached to the MyoStar catheter for transendocardial injection. The NOGA map was used for identification of injection locations, and 25 0.2-ml injections were performed throughout the LV free wall and septal wall. In the second animal, following anesthesia, an MI was given via deployment of 2 embolization coils as previously described (5,30). Two weeks later, an injection procedure was performed with the NOGA-guided MyoStar catheter as described earlier in the text. Fifteen 0.25-ml injections were performed in the infarct and border zone.

Histology and immunohistochemistry. For the rat studies, animals were euthanized with an overdose of sodium pentobarbital (200 mg/kg). Hearts were immediately removed, fresh frozen in Tissue Tek OCT freezing medium, and sectioned into 10-μm slices. Slides spaced approximately every 0.5 mm were stained with H&E for identification of infarcted tissue or for examination of inflammatory response by a pathologist blinded to the study. Immunohistochemistry (IHC) was performed on 5 slides from the infarct in each heart using the antibodies directed against the following antigens: Ki67 (Abcam, Cambridge, Massachusetts; 1:100), cardiac-specific troponin T (NeoMarkers, Fremont, California; 1:50), Connexin43 (Millipore, Temecula, California; 1:200), alpha smooth muscle actin (Dako, Carpinteria, California; 1:75), anti-CD163 (AbD Serotec, Raleigh, North Carolina; 1:50), and anti-c-Kit (Santa Cruz Biotechnology, Santa Cruz, California; 1:100). All primary antibodies were visualized by the addition of Alexa Fluor 568 and 488 (Invitrogen, Carlsbad, California) secondary antibodies. Sections that were stained with only the primary antibody or only the secondary antibody were used as negative controls. Sections were stained with Hoechst to visualize nuclei, and mounted with Fluoromount (Sigma, St. Louis, Missouri). Images were taken with a Carl Zeiss Observer D.1 (Carl Zeiss, Oberkochen, Germany) and analysis was performed by a blinded investigator with AxioVision software (Carl Zeiss) and Photoshop (Adobe Systems, San Jose, California). To assess retention and biodistribution of the myocardial matrix upon injection in a porcine model, the heart and satellite organs were removed for histological analysis. The pigs remained on anesthesia for 1 to 2 h following the injection surgery, before being euthanized with Fatal-Plus Solution (Vortech Pharmaceuticals, Dearborn, Michigan) at 0.22 ml/kg. This time frame was determined in the rat model to be adequate time to allow for gelation of the material within the myocardial tissue (16). Upon sacrifice, the heart was removed, with pericardium intact. Heart slices were fresh frozen using Tissue-Tek OCT compound for histological analysis, to locate the myocardial matrix. Five to 10 g of each of the following organs were collected to assess distribution to satellite organs as previously described for cell retention following catheter delivery (5,31): right and left lungs, liver, spleen, right and left kidneys, and right and left brain. Samples were frozen for histological analysis. The ventricular tissue and satellite organs were each sectioned into 10-μm sections and stained with H&E. Adjacent sections were stained for visualization of biotin-labeled myocardial matrix. Slides were fixed in acetone for 1.5 min, incubated with superblock buffer (30 min), followed by 3% hydrogen peroxide (30 min), and horseradish peroxidase–conjugated neutravidin (5 μg/ml, 30 min) at room temperature. The reaction was visualized by incubation with diaminobenzidine for 10 min. Sections from each organ were stained at the same time as the ventricular tissue, and images taken after 10 min of incubation.

Statistical analysis. Data are presented as mean $\pm$ standard error of the mean. MRI data pre- and post-treatment were assessed for each group using a paired *t* test. Changes in EF, ESV, and EDV, and IHC data were compared with a 2-sample *t* test. Significance was accepted at $p < 0.05$.

Results

Injectable myocardial matrix fabrication and characterization. We isolated ventricular ECM from fresh porcine ventricular myocardium (Fig. 1A) using SDS as previously described (16). After approximately 4 to 5 days in 1% SDS, cellular material was effectively removed, yielding white, translucent ventricular ECM (Fig. 1B). H&E sections of the decellularized ECM confirmed cell removal and lack of nuclei (Fig. 1C). The cardiac ECM was then lyophilized and milled into a powder (Fig. 1D), and finally solubilized with enzymatic digestion (Fig. 1E), thereby allowing for injection in subsequent studies (Fig. 1F).

To confirm the decellularized myocardial ECM retained the proteins and proteoglycans native to the myocardium, myocardial matrix powder was characterized using LC-MS/MS. LC-MS/MS revealed a variety of ECM proteins, indicating retained protein content after decellularization. The ECM proteins, glycoproteins, and proteoglycans iden-

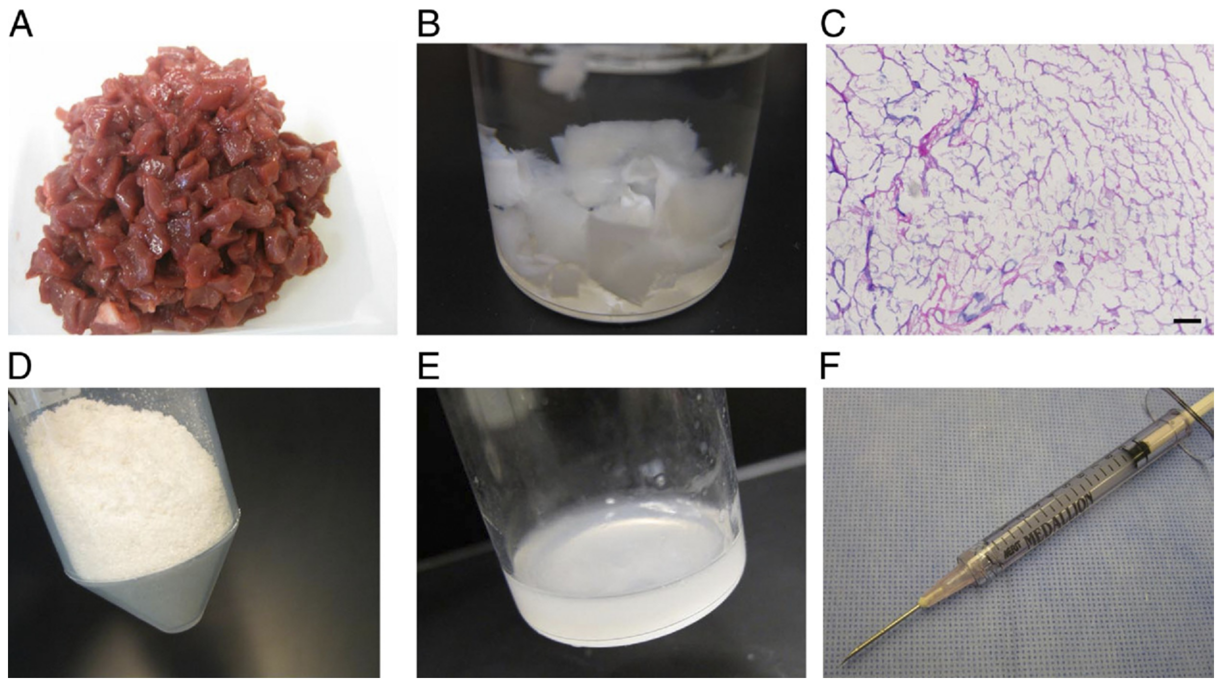

Figure 1 **Myocardial Matrix Fabrication**

(A) Porcine ventricular myocardium is sliced and then **(B)** decellularized using sodium dodecyl sulfate. **(C)** Hematoxylin and eosin staining of a histological section reveals cellular removal. The decellularized extracellular matrix is then milled into a fine powder **(D)** and then solubilized through enzymatic digestion **(E)**, which allows for injection via syringe and a 27-gauge needle **(F)**.

tified included: collagen types I, III, IV, V, and VI, elastin, fibrinogen, lumican, perlecan, fibulin, and laminin. Collagen, laminin, and elastin are the major ECM proteins, responsible for structure. Perlecan, a heparin sulfate proteoglycan associated with vascularized tissues, is known to promote adhesion and basic fibroblast growth factor receptor binding, as well as plays a role in developmental and remodeling processes, such as angiogenesis (32–34). Fibulin, a calcium-binding glycoprotein, commonly associates with other ECM components such as fibronectin (35,36). The identification of these components within the decellularized and processed myocardial matrix indicates a retained complex combination of proteins and proteoglycans, important for a biomimetic tissue engineering scaffold. It should, however, be noted that mass spectrometry is not an all-inclusive technique, and therefore, other proteins may not have been identified.

Arrhythmia inducibility. Numerous materials have been injected into infarcted rodent myocardium to date, yet no studies have directly assessed safety in terms of a potential for arrhythmias, which has been a concern with cell injections (3,37–39). We therefore assessed arrhythmia inducibility using programmed electrical stimulation in vivo by burst and extrastimulus pacing protocols in rats 1 week post-injection of myocardial matrix ($n = 20$) compared to saline ($n = 16$). We chose to examine 1 week post-injection because the material is still present in the tissue at this time. In vivo pacing protocols (23–25) induced nonsustained VT (monomorphic or polymorphic, self-terminating VT) in 37.5% of saline-injected hearts and 35% of matrix-injected hearts. Sustained VT (>30 s) was induced once during burst pacing in a matrix-injected rat (5% occurrence rate), and once during extrastimulus pacing in a saline-injected rat (6.25% occurrence rate). No statistical significance was found when comparing the average incidence of VT between groups ($p = 0.8$) (Fig. 2).

Histological and immunohistochemical analysis. To examine the local tissue response to myocardial matrix injection, a subset of animals utilized in the arrhythmia studies were utilized for histological and immunohistochemical analysis ($n = 5$ each group). Histological assessment of infarcts 1 week post-injection showed an increased cellular infiltration response in myocardial matrix injection animals. There was a moderate mononuclear cell infiltration response with predominantly lymphocytes and some macrophages (Fig. 3A). Additional spindle-shaped cells were also observed, likely indicating some fibroblast infiltration. There was no indication of matrix encapsulation or rejection. We further performed IHC on the heart sections with antibodies for markers for cardiomyocytes (troponin), M2 macrophages (CD163), and proliferative cells (Ki67). Striking differences were observed in the size of cardiomyocyte islands surviving within the infarct region in matrix-injected hearts, and we thus quantified the area of these regions

JACC Vol. 59, No. 8, 2012
February 21, 2012:751–63

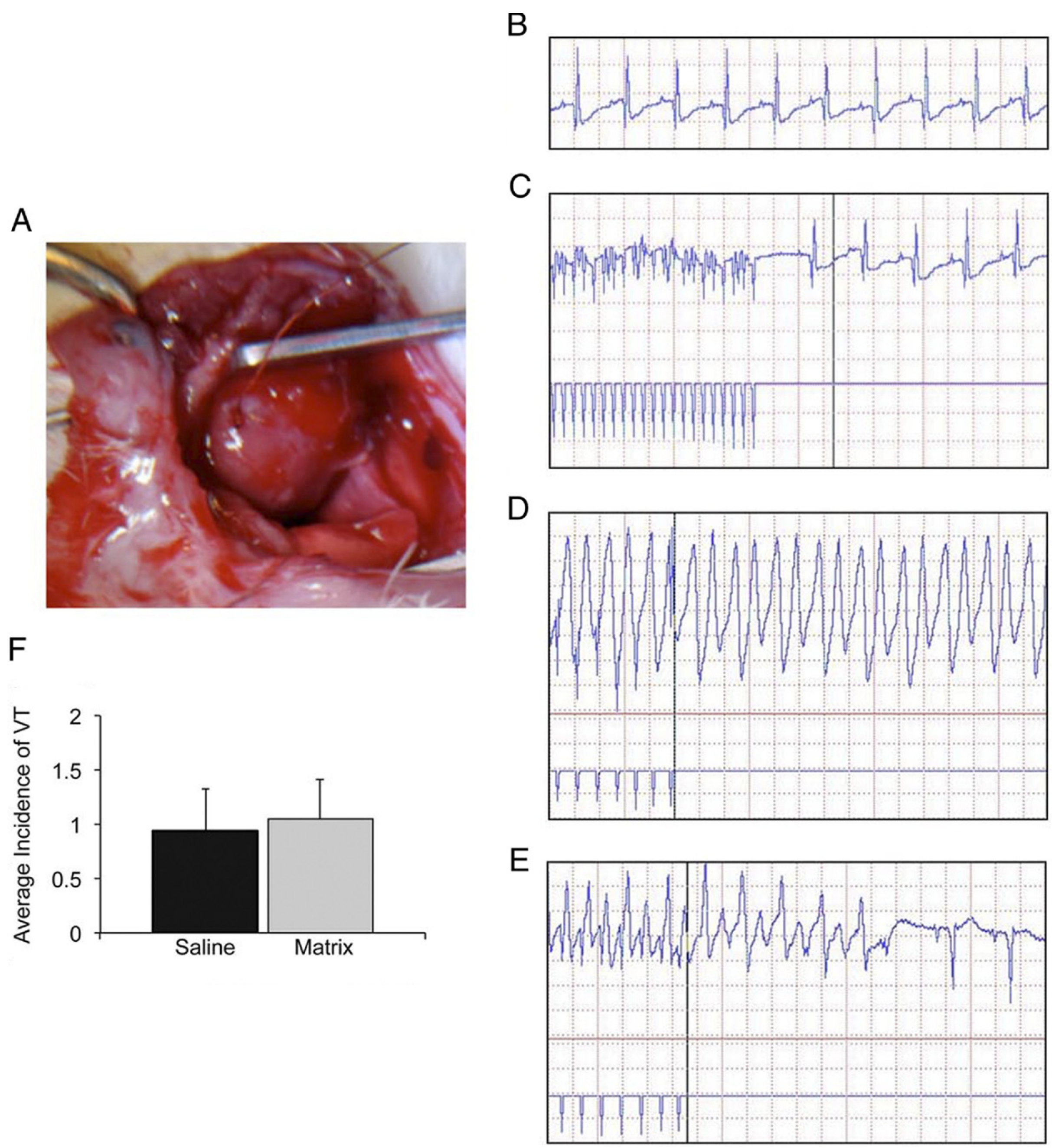

Figure 2 **Programmed Electrical Stimulation to Assess Potential for Arrhythmogenesis**

(A) An electrode paces the left ventricle of rat hearts 1 week post-injection. **(B)** Intrinsic rhythm of rat heart prior to pacing. **(C)** Return to intrinsic rhythm when burst pacing is stopped. **(D)** Sustained ventricular tachycardia (VT) following a single extrastimulus. **(E)** Nonsustained VT following a single extrastimulus. **(F)** There was no observed difference in the average incidence of VT between saline and myocardial matrix groups, demonstrating that the myocardial matrix hydrogel is not proarrhythmogenic.

compared with controls. The average area of these islands of viable myocardium within the infarct of matrix-injected hearts (0.05 $\pm$ 0.01 mm^2) was statistically larger than the average area of those within the infarct of saline-injected hearts (0.03 $\pm$ 0.01 mm^2, matrix, $p = 0.045$) (Fig. 3B). Within these regions of viable myocardium, positive staining for Connexin 43 was observed (not shown), indicating the presence of gap junctions. Although quantification of M2 macrophages within the infarct was not significantly significant between groups ($p = 0.2$) (Fig. 3C), matrix-

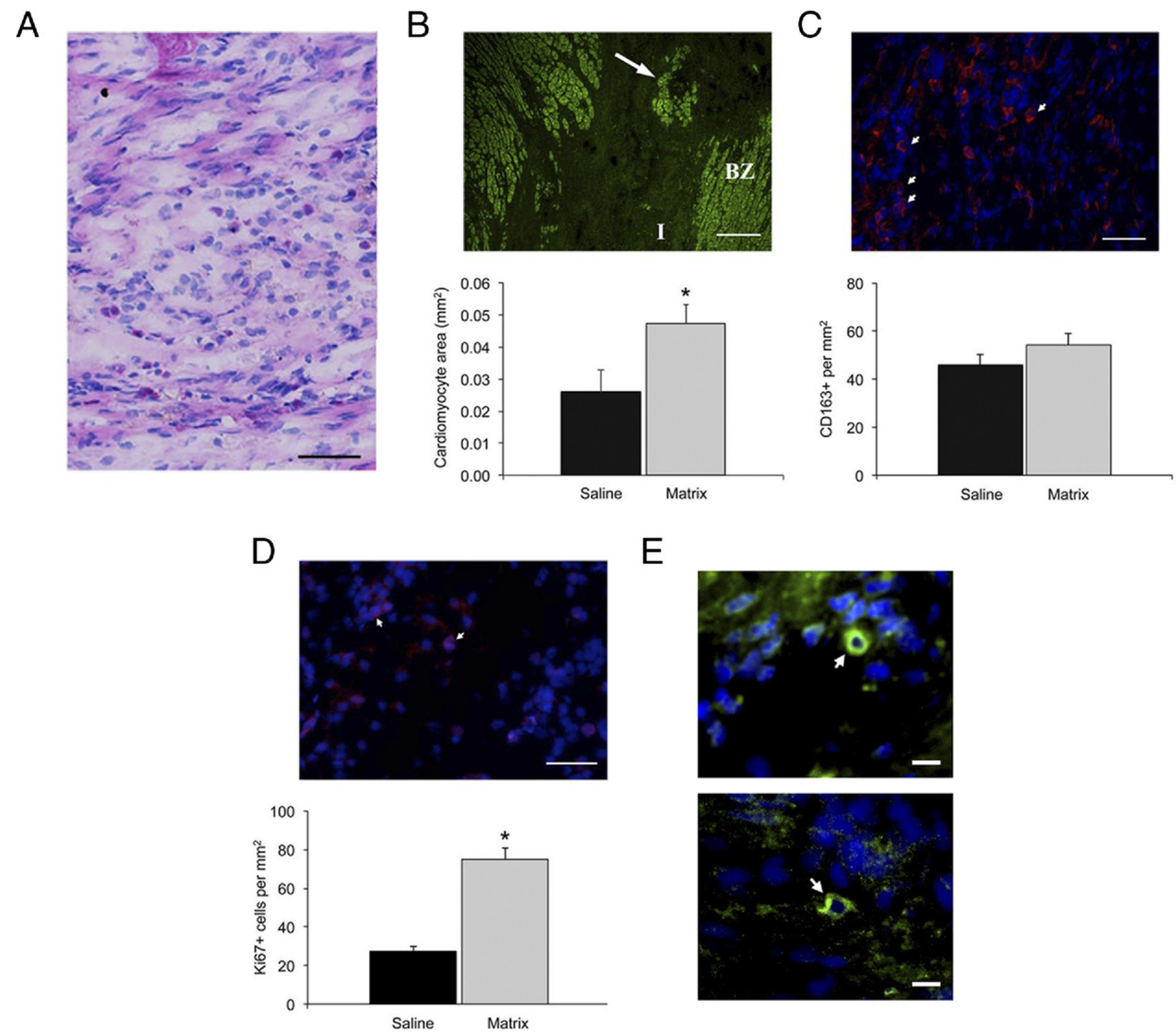

Figure 3 **Histological and Immunohistochemical Assessment**

(A) Hematoxylin and eosin staining of matrix-injected infarct demonstrating moderate mononuclear cell infiltration (scale bar = 50 μm). **(B)** An increased average area of cardiomyocyte islands were found in the infarct of myocardial matrix–injected hearts compared with saline controls (*$p < 0.05$). An island of viable myocardium in the infarct of a matrix-injected heart is denoted by the **arrow** (scale bar = 200 μm). Cardiac troponin T is shown in **green** with the infarct and border zone denoted by I and BZ, respectively. **(C)** There was no significant difference in the number of infiltrating M2 macrophages between groups. Nuclei are stained **blue** with Hoechst, and CD163$^+$ cells are labeled **red**, with a few cells denoted by the **arrow points** (scale bar = 100 μm). **(D)** An increase in proliferative cells were observed in matrix-injected hearts (*$p < 0.05$). Nuclei are stained **blue** with Hoechst, and Ki67$^+$ cells are labeled **red**. Co-stained nuclei appear **purple**, with a couple cells denoted by **arrow points** (scale bar = 50 μm). **(E)** C-kit$^+$ cells were observed in low numbers within the myocardial matrix scaffold. C-kit$^+$ cells (denoted with **arrow points**) are labeled in **green**, with nuclei in **blue** (scale bar = 10 μm).

injected hearts did show a significantly higher density of proliferative cells (saline: 27.6 ± 6.8 per mm^2, matrix: 75.1 ± 18 per mm^2, $p = 0.039$) (Fig. 3D). Many of the Ki67$^+$ cells had a rounded/oval nuclei shape, which is indicative of lymphocytes. Co-staining of Ki67 and troponin revealed that only ~1% of Ki67-positive cells were proliferating cardiomyocytes. Additional slides, co-stained for Ki67 and alpha smooth muscle actin, identified that myofibroblasts were proliferative within matrix-injected hearts, but were not quantified, due to low numbers. We also examined matrix-injected regions for the presence of c-kit$^+$ cells, which are progenitor cells that have been shown to differentiate into myocardial precursors and vascular cells in the heart (40,41). C-kit$^+$ cells were observed within the myocardial matrix scaffold (Fig. 3E); however, they were in low numbers.

Preservation of cardiac function post-MI. MRI (Figs. 4A to 4D) was used to measure LV EDV, ESV, and EF at 1 week post-MI (1 week prior to injection) and 6 weeks post-MI (4 weeks post-injection) to evaluate effects of myocardial matrix injections on cardiac function (Table 2). As expected, the EF (Fig. 4E) of saline-injected hearts ($n = 6$) significantly declined, whereas both the ESV

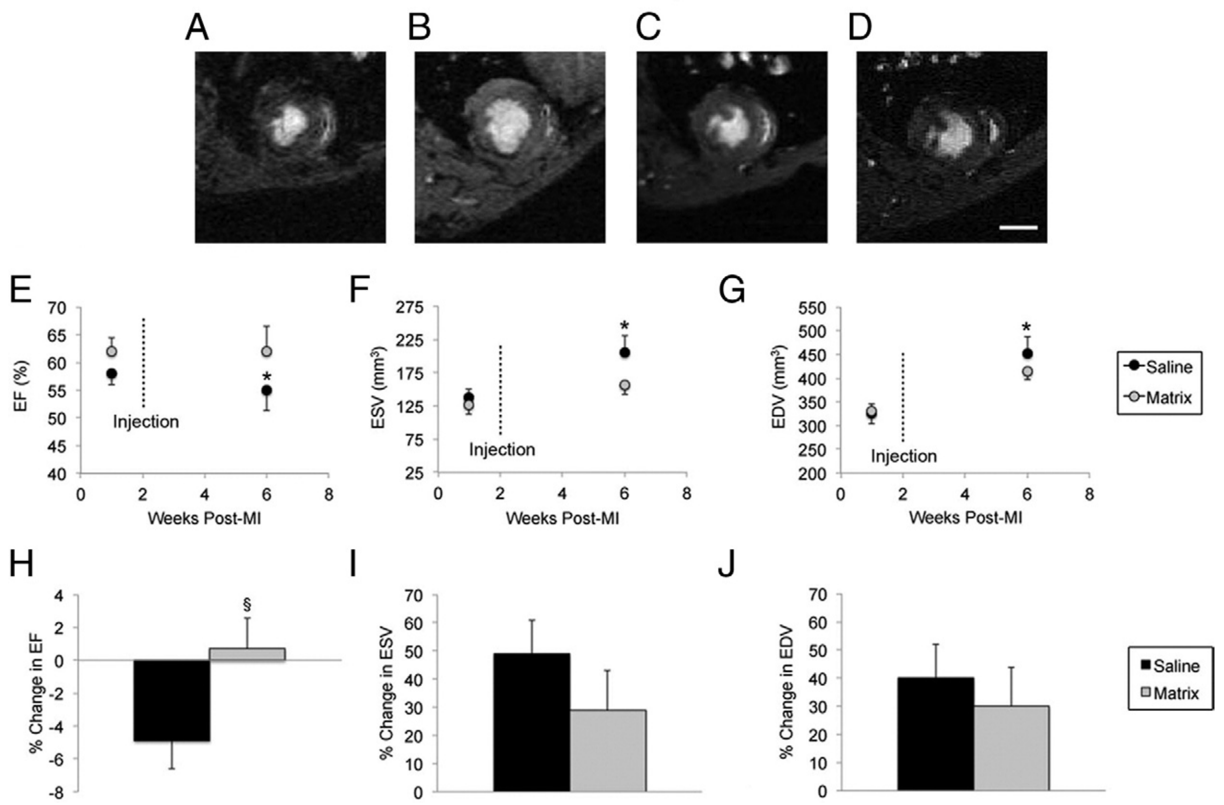

Figure 4 **MRI Analysis in Rat MI Model**

(A) Baseline (1 week post-myocardial infarction [MI], 1 week pre-injection) and **(B)** 4 weeks post-injection images of saline-injected heart. **(C)** Baseline and **(D)** 4 weeks post-injection images of myocardial matrix–injected heart. Scale bar = 0.5 cm. **(E)** Ejection fraction (EF) of saline controls significantly declined ($p = 0.04$), whereas the **(F)** end-systolic volume (ESV) ($p = 0.01$) and **(G)** end-diastolic volume (EDV) ($p = 0.01$) significantly expanded between 1 week and 6 weeks post-MI. By contrast, there was no statistical significance for EF ($p = 0.8$), ESV ($p = 0.054$), and EDV ($p = 0.06$) between time points in the myocardial matrix group. Myocardial matrix–injected animals had an overall increase in the percent change in EF (§$p = 0.054$) **(H)**, and overall decrease in the percent change in volume **(I and J)** between time points compared to saline, although these were not statistically significant. Data are presented as the mean ± SEM; *$p < 0.05$. MRI = magnetic resonance imaging.

(Fig. 4F) and EDV (Fig. 4G) significantly expanded. In contrast, there was no statistical significance between EF, ESV, and EDV of myocardial matrix–injected animals ($n = 6$) (Figs. 4E to 4G) despite injections being performed 1 week after baseline imaging. When comparing the percent change in EF, ESV, and EDV between groups, myocardial matrix–injected animals had an increase in EF (Fig. 4B), and a relative decrease in percent change in ESV (Fig. 4I) and EDV (Fig. 4J) compared with controls, although these were not significant.

Percutaneous transendocardial delivery of myocardial matrix. The liquid myocardial matrix was tested for clinical feasibility using a MyoStar Intramyocardial Injection device for transendocardial delivery, a technique that has been employed for minimally invasive delivery for cellular cardiomyoplasty (4,5,9). Prior to injection, a unipolar electromechanical map (NOGA) was created to allow for selection of injection sites. Matrix was prepared as described in the previous text, loaded into a 1-ml syringe for connection to the catheter (Fig. 5A), and injections were made via

Table 2 **MRI Data**

	Saline			Matrix		
	1 Week Pre-Injection (1 Week Post-MI)	4 Weeks Post-Injection (6 Week Post-MI)	% Change	1 Week Pre-Injection (1 Week Post-MI)	4 Weeks Post-Injection (6 Week Post-MI)	% Change
EF, %	58.0 ± 2.4	55.0 ± 4.5*	−4.9 ± 0.7	62.0 ± 2.0	62.0 ± 3.7	0.7 ± 1.9
ESV, mm^3	137 ± 13	205 ± 25*	49 ± 12	126 ± 14	157 ± 15	29 ± 14
EDD, mm^3	325 ± 20	451 ± 37*	40 ± 12	331 ± 27	414 ± 18	30 ± 14

Values are mean ± SEM. *$p < 0.05$ compared with baseline.
EDD = end-diastolic dimension; EF = ejection fraction; ESV = end-systolic volume; MRI = magnetic resonance imaging.

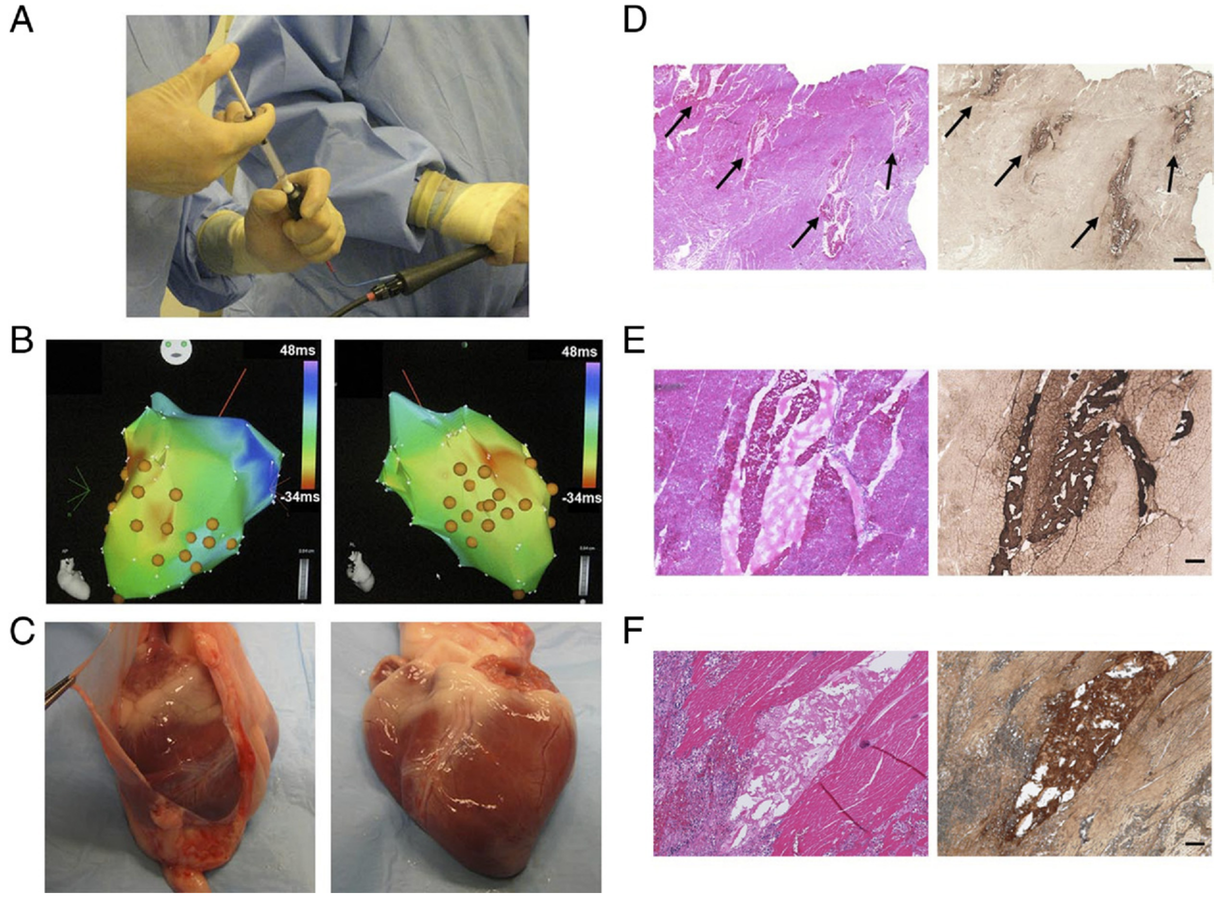

Figure 5 **Percutaneous Transendocardial Delivery of Myocardial Matrix Hydrogel**

(A) Image of myocardial matrix being injected through a MyoStar 27-gauge catheter, using a 1-ml Luer lock syringe, attached to the catheter. **(A and B)** NOGA maps for healthy animal representing final injection locations, indicated by **orange dots**. **(C)** Upon heart excision 2 h post-injection, there were no signs of pericardial effusion. **(D and E)** Hematoxylin and eosin (H&E) **(left)** and diaminobenzidine **(right)** staining of left ventricular free wall showing gelled myocardial matrix within healthy myocardium. Multiple injection locations are shown in **D**, indicated by **arrows**. **(F)** H&E **(left)** and DAB **(right)** staining of myocardial matrix scaffold in infarcted myocardium. Scale bars = 1 mm, 100 μm, and 100 μm in **D**, **E**, and **F**, respectively.

endoventricular catheter delivery using the MyoStar Intramyocardial needle-injection catheter. Successful transendocardial delivery of liquid myocardial matrix into 25 injection sites (0.2 ml each site) throughout the septal wall and LV free wall was achieved in the healthy animal, and 15 injections (0.25 ml each site) were achieved in the infarct and border zone of the infarcted animal, with no sustained arrhythmias during or after the injection procedures. The material remained injectable during the approximately 1-h-long procedures, without premature gelation or clogging of the catheter. The location of each individual injection was guided and documented through the use of NOGA mapping (Fig. 5B). One to 2 h after injection of myocardial matrix via transendocardial catheter delivery, the animals were euthanized and the hearts removed. By gross observation, there were no signs of pericardial effusion (Fig. 5C). Detection of the matrix within the LV free wall (Figs. 5D and 5E) and septal wall of the healthy animal and within the infarct area in the MI animal (Fig. 5F), confirmed successful delivery into the myocardium, as well as gelation of the matrix in vivo. As with any intramyocardial injection technique, there is a concern that the injected material will leak into the ventricle and travel through the blood stream to other organs. Thus, the lungs, kidney, brain, liver, and spleen were also examined; no myocardial matrix was observed in any of the satellite organs.

Discussion

This work establishes proof-of-concept for the clinical feasibility of the recently developed myocardial matrix as an injectable biomaterial for treating MI through a minimally invasive approach. Herein, we show that this injectable scaffold preserves cardiac function in a small animal model. We further demonstrate that the material can be successfully delivered via a percutaneous transendocardial approach into the ventricular wall in both healthy and infarcted porcine myocardium.

Although developing a therapy from porcine tissue helps to eliminate the need for human organ donation, there is potential concern associated with the immunogenicity of a xenogeneic material. Previous studies, however, have shown that xenogeneic decellularized ECMs are biocompatible, and many have been approved by the Food and Drug Administration and used successfully in the clinic (42). We nonetheless examined the local tissue response to the porcine-derived myocardial matrix hydrogel. The mononuclear infiltrate seen here is similar to that seen in previous studies that show the immune response of decellularized small intestine submucosa ECM as being comparable to syngeneic muscle implants, rather than eliciting foreign-body giant cell formation and encapsulation, indicative of rejection seen with xenogeneic implantation (43,44). Furthermore, small intestine submucosa ECM implantation resulted in an increase of cytokines that are known to be produced by a subset of lymphocytes, Th2 cells, which are associated with a normal immune response and graft acceptance (45,46). Thus, the presence of lymphocytes within the infarcted tissue of the myocardial matrix–injected hearts corroborates that the myocardial matrix is able to elicit an immune response typical of decellularized matrices, and suggests a potentially positive impact on the infarct environment, as the Th2 response that predominates with decellularized ECMs results in the production of anti-inflammatory cytokines (43,44). We also found an increase in proliferating cells, suggesting the matrix affects the proliferation of cells within the infarct, as was also seen upon injection of a small intestine submucosa emulsion (47). Although many of the cells were lymphocytes, we also co-stained for cardiomyocytes and myofibroblasts. The heart is known to have limited regenerative capacity, yet cardiomyocytes have been shown to proliferate in the failing heart (48). However, only $\sim$1% of Ki67^{+} cells were co-stained for troponin. A small subset of proliferating cells were also identified as myofibroblasts, which are thought to be critical in the remodeling process post-MI (49). We further observed the presence of c-kit^{+} cells within the matrix scaffold; however, they were in low numbers.

A variety of materials have been explored as injectable therapies for cardiac repair post-MI, and have shown preserved or improved cardiac function (12–14,50). However, the recently developed myocardial matrix is naturally derived from decellularized porcine ventricular tissue and is therefore uniquely able to offer properties of the native cardiac ECM. A material that mimics the microenvironment of native ECM structurally and biochemically is important in any tissue engineering application, as it allows for appropriate cell–matrix interactions (51,52). Natively, these interactions are specific for each tissue, with each ECM having its own distinct combination of proteins and proteoglycans (51,53). The myocardial matrix has been shown, through gel electrophoresis and glycosaminoglycan quantification (16), as well as mass spectrometry analysis, to retain a complexity of ventricular ECM proteins, peptides, and polysaccharides, making it a cardiac-specific scaffold for myocardial tissue engineering. This tissue specificity may provide benefits over non–tissue-matched decellularized matrices. For example, a previous study utilizing decellularized urinary bladder matrix as a ventricular patch lead to the presence of cartilaginous tissue (54), which may have been the result of non–tissue-specific cues.

Here, we also show an increase in the size of cardiomyocyte islands surviving in the infarct area, which, to the best of our knowledge, has not been previously reported with other material injections. Although most cardiomyocytes undergo apoptosis or necrosis soon after the induction of MI, and cell death peaks 4 days post-MI, additional waves of cardiomyocyte death continue for weeks or months (55). Thus, the retained areas of cardiomyocytes suggest that matrix injection may act to salvage remaining cardiomyocytes, or prevent the further necrosis. Furthermore, gap junctions, identified by Connexin 43 staining, were present among these cells, suggesting electrical conductance within the cardiomyocyte clusters. In addition to local effects on endogenous cell types, a cardiac-specific scaffold may also have key benefits for transplant cell delivery because the biochemical cues in the myocardial matrix have been recently shown in vitro to promote enhanced maturation of human embryonic stem cell–derived cardiomyocytes (56).

We demonstrate that injection of the myocardial matrix hydrogel preserves cardiac function post-MI in a rodent model; however, the exact mode of action behind the improvement for this hydrogel as well as other injectable materials has not yet been fully elucidated (57). A recent study in our lab, which showed that an inert nondegradable synthetic material did not affect cardiac function post-MI, suggests that biological cues or cell infiltration as a result of material degradation may play important roles in preserving/improving LV function (58). In this study, we show the myocardial matrix results in an influx of cells typical of decellularized ECM materials, which includes lymphocytes. As stated in previous text, a Th2 response, as seen with decellularized ECMs, results in the production of anti-inflammatory cytokines, including interleukin (IL)-10 (43,44). IL-10 has been shown to inhibit LV remodeling and improve function post-MI (59), and therefore may also be a potential mode of action here. We have previously shown that the myocardial specific biochemical cues in the myocardial matrix promote maturation of human embryonic stem cell derived cardiomyocytes in vitro (56). In this study, we saw an increase in the size of surviving islands of viable myocardium within the infarct. This result may be due to the presence of myocardial specific cues in the myocardial matrix; however, the material on its own does not appear to result in significant regeneration because we only saw low numbers of c-kit^{+} cells within the scaffold. Although a material-alone therapy would facilitate translation, a combination therapy may be needed to promote regeneration.

A safety issue that has arisen with intramyocardial injections is the potential for arrhythmogenesis. Although many studies have examined injectable materials for treating MI in rodent models, none have directly assessed whether injection of these materials increases arrhythmias. We therefore performed programmed electrical stimulation studies 1 week post-injection in the rat model as well as monitored the ECG up to 2 h post-injection in the porcine model. We did not observe an increase in incidences of arrhythmia with injection of the myocardial matrix hydrogel. Our results, along with 2 recent reports of material injections in porcine models (through intracoronary infusion [15] and intramyocardial injection [60]), suggest that material delivery into the infarct area does not lead to induced arrhythmogenesis. However, material degradation and scar maturation over time may lead to electrophysiological changes, and therefore, it will be critical to assess multiple time points for a given material in a large animal model prior to clinical translation.

Several materials investigated for injectable therapy, including fibrin glue (13,21), collagen (14), chitosan (61), Matrigel (62), and hyaluronic acid (63) have demonstrated preserved or improved cardiac function, yet may not translate to catheter delivery in the heart, which would limit their relevance for minimally invasive treatment in humans. For an injectable material to be clinically relevant for percutaneous delivery in the heart, the material must remain liquid, with an appropriate viscosity for delivery of multiple injections through a catheter, and convert to a gel once it is within the myocardial tissue. Although several materials have shown promising results in small animals, few have actually been translated to percutaneous delivery in large animals. Recently, alginate (15) was delivered through intracoronary injection in large animals. However, endocardial delivery, commonly used for cellular cardiomyoplasty (4,5,9,15,64,65), is considered to be the preferred method of catheter delivery in terms of retention (66–68), because it allows for direct intramyocardial delivery and does not require access to the coronary vessels. In addition, the guarantee of migration into the myocardium is uncertain with intracoronary delivery, and there is a risk of microembolism (69). Here, we show that the myocardial matrix hydrogel preserves cardiac function post-MI in a rat model, and also demonstrate that it is deliverable via catheter in a porcine model. The myocardial matrix was successfully injected via a percutaneous, transendocardial approach in both healthy and infarcted porcine myocardium without clogging the catheter. It should, however, be noted that some leakage of injectate into the ventricle is known to occur with transendocardial delivery (5,31). Any myocardial matrix that leaks into the ventricle would likely be rapidly diluted in the blood, thereby preventing gelation. We confirmed through histological analysis that the myocardial matrix formed a hydrogel within the porcine myocardial tissue without measurable embolization in other organs. It is, however, possible that a small amount of material was present in other organs and below our detection limit.

Study limitations. First, injections were performed 2 weeks post-MI, an entire week after the baseline MRI analysis. Because of this delay between baseline measurements and treatment injection, the LV volume likely continued to increase prior to injection, which is indicated by the data (Fig. 4). Therefore, it is unknown if this decrease would occur if injections had been performed immediately post baseline imaging. Second, LV remodeling is well underway at the injection time point of 2 weeks post-MI, and injection of the myocardial matrix shortly after MI, at which time the native ECM has been recently degraded, may have enhanced effects. However, we chose to inject at a later time point as it is more clinically relevant than injection immediately post-MI when there is a significant risk of ventricular rupture. Last, although we examined catheter delivery in a large animal, the majority of this study is in a rat myocardial infarction model. Inherent limitations with this model include the inability to precisely control injections and, therefore, the inability to homogenously cover the entire infarct area. Examining functional changes in a large animal MI model will be critical prior to clinical translation.

Conclusions

Although a variety of materials have shown success in small animal models (12–14,50), the myocardial matrix not only preserves cardiac function in a rat model, without inducing arrythmias, but also shows initial translation to large animals. Specifically, we have shown clinical feasibility of the myocardial matrix for minimally invasive delivery, by demonstrating transendocardial catheter delivery and retention within the myocardium. The myocardial matrix is the first material to be designed as a tissue-specific, injectable scaffold for cardiac tissue engineering, and is to our knowledge the first in situ gelling material to be injected via percutaneous transendocardial delivery. Our results warrant further study of this material in a large animal MI model and demonstrate the potential of this technology for treating patients with MI.

Acknowledgments
The authors thank Carolina Rogers, Dr. Majid Ghassemian, and Dr. Kent Osborne for assistance with porcine tissue collection, mass spectrometry, and histological assessment, respectively. In addition, they would like to acknowledge Timothy Salazar and Dr. Miriam Scadeng of the fMRI center, as well as Dr. Joyce Chuang for MRI guidance. They also thank Dr. Adam Wright and Aboli Rane for assistance with pacing studies, and Biologics Delivery Systems for providing NOGA mapping support.

Reprint requests and correspondence: Dr. Karen L. Christman, University of California, 9500 Gilman Drive, MC 0412, La Jolla, California 92093. E-mail: christman@bioeng.ucsd.edu.

REFERENCES

1. Lloyd-Jones D, Adams R, Carnethon M, et al. Heart disease and stroke statistics—2009 update: a report from the American Heart Association Statistics Committee and Stroke Statistics Subcommittee. Circulation 2009;119:480–6.
2. Mann DL. Mechanisms and models in heart failure: a combinatorial approach. Circulation 1999;100:999–1008.
3. Smits PC, van Geuns RJ, Poldermans D, et al. Catheter-based intramyocardial injection of autologous skeletal myoblasts as a primary treatment of ischemic heart failure: clinical experience with six-month follow-up. J Am Coll Cardiol 2003;42:2063–9.
4. Dib N, Diethrich EB, Campbell A, et al. Endoventricular transplantation of allogenic skeletal myoblasts in a porcine model of myocardial infarction. J Endovasc Ther 2002;9:313–9.
5. Dib N, Campbell A, Jacoby DB, et al. Safety and feasibility of percutaneous autologous skeletal myoblast transplantation in the coil-infarcted swine myocardium. J Pharmacol Toxicol Methods 2006;54:71–7.
6. Fuchs S, Kornowski R, Weisz G, et al. Safety and feasibility of transendocardial autologous bone marrow cell transplantation in patients with advanced heart disease. Am J Cardiol 2006;97:823–9.
7. Fuchs S, Satler LF, Kornowski R, et al. Catheter-based autologous bone marrow myocardial injection in no-option patients with advanced coronary artery disease: a feasibility study. J Am Coll Cardiol 2003;41:1721–4.
8. Dib N, Michler RE, Pagani FD, et al. Safety and feasibility of autologous myoblast transplantation in patients with ischemic cardiomyopathy: four-year follow-up. Circulation 2005;112:1748–55.
9. Perin EC, Dohmann HF, Borojevic R, et al. Transendocardial, autologous bone marrow cell transplantation for severe, chronic ischemic heart failure. Circulation 2003;107:2294–302.
10. Davis ME, Hsieh PC, Grodzinsky AJ, Lee RT. Custom design of the cardiac microenvironment with biomaterials. Circ Res 2005;97:8–15.
11. Christman KL, Lee RJ. Biomaterials for the treatment of myocardial infarction. J Am Coll Cardiol 2006;48:907–13.
12. Landa N, Miller L, Feinberg MS et al. Effect of injectable alginate implant on cardiac remodeling and function after recent and old infarcts in rat. Circulation 2008;117:1388–96.
13. Christman KL, Fok HH, Sievers RE, Fang Q, Lee RJ. Fibrin glue alone and skeletal myoblasts in a fibrin scaffold preserve cardiac function after myocardial infarction. Tissue Eng 2004;10:403–9.
14. Dai W, Wold LE, Dow JS, Kloner RA. Thickening of the infarcted wall by collagen injection improves left ventricular function in rats: a novel approach to preserve cardiac function after myocardial infarction. J Am Coll Cardiol 2005;46:714–9.
15. Leor J, Tuvia S, Guetta V, et al. Intracoronary injection of in situ forming alginate hydrogel reverses left ventricular remodeling after myocardial infarction in Swine. J Am Coll Cardiol 2009;54:1014–23.
16. Singelyn JM, DeQuach JA, Seif-Naraghi SB, Littlefield RB, Schup-Magoffin PJ, Christman KL. Naturally derived myocardial matrix as an injectable scaffold for cardiac tissue engineering. Biomaterials 2009;30:5409–16.
17. Ott HC, Matthiesen TS, Goh SK, et al. Perfusion-decellularized matrix: using nature's platform to engineer a bioartificial heart. Nat Med 2008;14:213–21.
18. Singelyn JM, Christman KL. Injectable materials for the treatment of myocardial infarction and heart failure: the promise of decellularized matrices. J Cardiovasc Transl Res 2010;3:478–86.
19. Freytes DO, Martin J, Velankar SS, Lee AS, Badylak SF. Preparation and rheological characterization of a gel form of the porcine urinary bladder matrix. Biomaterials 2008;29:1630–7.
20. Villarreal FJ, Griffin M, Omens J, Dillmann W, Nguyen J, Covell J. Early short-term treatment with doxycycline modulates postinfarction left ventricular remodeling. Circulation 2003;108:1487–92.
21. Christman KL, Vardanian AJ, Fang Q, Sievers RE, Fok HH, Lee RJ. Injectable fibrin scaffold improves cell transplant survival, reduces infarct expansion, and induces neovasculature formation in ischemic myocardium. J Am Coll Cardiol 2004;44:654–60.
22. Huang NF, Sievers RE, Park JS, Fang Q, Li S, Lee RJ. A rodent model of myocardial infarction for testing the efficacy of cells and polymers for myocardial reconstruction. Nat Protoc 2006;1:1596–609.
23. Schrickel JW, Bielik H, Yang A, et al. Induction of atrial fibrillation in mice by rapid transesophageal atrial pacing. Basic Res Cardiol 2002;97:452–60.
24. Roell W, Lewalter T, Sasse P, et al. Engraftment of connexin 43-expressing cells prevents post-infarct arrhythmia. Nature 2007;450:819–24.
25. Kreuzberg MM, Schrickel JW, Ghanem A, et al. Connexin30.2 containing gap junction channels decelerate impulse propagation through the atrioventricular node. Proc Natl Acad Sci U S A 2006;103:5959–64.
26. Costandi PN, Frank LR, McCulloch AD, Omens JH. Role of diastolic properties in the transition to failure in a mouse model of the cardiac dilatation. Am J Physiol Heart Circ Physiol 2006;291:H2971–9.
27. Costandi PN, McCulloch AD, Omens JH, Frank LR. High-resolution longitudinal MRI of the transition to heart failure. Magn Reson Med 2007;57:714–20.
28. Nahrendorf M, Hiller KH, Hu K, Ertl G, Haase A, Bauer WR. Cardiac magnetic resonance imaging in small animal models of human heart failure. Med Image Anal 2003;7:369–75.
29. Kachenoura N, Redheuil A, Balvay D, et al. Evaluation of regional myocardial function using automated wall motion analysis of cine MR images: contribution of parametric images, contraction times, and radial velocities. J Magn Reson Imaging 2007;26:1127–32.
30. Dib N, Diethrich EB, Campbell A, Gahremanpour A, McGarry M, Opie SR. A percutaneous swine model of myocardial infarction. J Pharmacol Toxicol Methods 2006;53:256–63.
31. Freyman T, Polin G, Osman H, et al. A quantitative, randomized study evaluating three methods of mesenchymal stem cell delivery following myocardial infarction. Eur Heart J 2006;27:1114–22.
32. Aviezer D, Hecht D, Safran M, Eisinger M, David G, Yayon A. Perlecan, basal lamina proteoglycan, promotes basic fibroblast growth factor-receptor binding, mitogenesis, and angiogenesis. Cell 1994;79:1005–13.
33. Whitelock JM, Graham LD, Melrose J, Murdoch AD, Iozzo RV, Underwood PA. Human perlecan immunopurified from different endothelial cell sources has different adhesive properties for vascular cells. Matrix Biol 1999;18:163–78.
34. Iozzo RV. Perlecan: a gem of a proteoglycan. Matrix Biol 1994;14:203–8.
35. Argraves WS, Dickerson K, Burgess WH, Ruoslahti E. Fibulin, a novel protein that interacts with the fibronectin receptor beta subunit cytoplasmic domain. Cell 1989;58:623–9.
36. Argraves WS, Tran H, Burgess WH, Dickerson K. Fibulin is an extracellular matrix and plasma glycoprotein with repeated domain structure. J Cell Biol 1990;111:3155–64.
37. Fernandes S, Amirault JC, Lande G, et al. Autologous myoblast transplantation after myocardial infarction increases the inducibility of ventricular arrhythmias. Cardiovasc Res 2006;69:348–58.
38. Kolettis TM. Arrhythmogenesis after cell transplantation post-myocardial infarction. Four burning questions—and some answers. Cardiovasc Res 2006;69:299–301.
39. Menasche P, Hagege AA, Vilquin JT, et al. Autologous skeletal myoblast transplantation for severe postinfarction left ventricular dysfunction. J Am Coll Cardiol 2003;41:1078–83.
40. Beltrami AP, Barlucchi L, Torella D, et al. Adult cardiac stem cells are multipotent and support myocardial regeneration. Cell 2003;114:763–76.
41. Limana F, Zacheo A, Mocini D, et al. Identification of myocardial and vascular precursor cells in human and mouse epicardium. Circ Res 2007;101:1255–65.
42. Badylak SF, Freytes DO, Gilbert TW. Extracellular matrix as a biological scaffold material: structure and function. Acta Biomater 2009;5:1–13.
43. Allman AJ, McPherson TB, Badylak SF, et al. Xenogeneic extracellular matrix grafts elicit a TH2-restricted immune response. Transplantation 2001;71:1631–40.
44. Allman AJ, McPherson TB, Merrill LC, Badylak SF, Metzger DW. The Th2-restricted immune response to xenogeneic small intestinal submucosa does not influence systemic protective immunity to viral and bacterial pathogens. Tissue Eng 2002;8:53–62.
45. Krenger W, Ferrara JL. Graft-versus-host disease and the Th1/Th2 paradigm. Immunol Res 1996;15:50–73.

46. Singh VK, Mehrotra S, Agarwal SS. The paradigm of Th1 and Th2 cytokines: its relevance to autoimmunity and allergy. Immunol Res 1999;20:147–61.
47. Zhao ZQ, Puskas JD, Xu D, et al. Improvement in cardiac function with small intestine extracellular matrix is associated with recruitment of C-kit cells, myofibroblasts, and macrophages after myocardial infarction. J Am Coll Cardiol 2010;55:1250–61.
48. Beltrami AP, Urbanek K, Kajstura J, et al. Evidence that human cardiac myocytes divide after myocardial infarction. N Engl J Med 2001;344:1750–7.
49. Jugdutt BI. Ventricular remodeling after infarction and the extracellular collagen matrix: when is enough enough? Circulation 2003;108:1395–403.
50. Wang T, Wu DQ, Jiang XJ, et al. Novel thermosensitive hydrogel injection inhibits post-infarct ventricle remodelling. Eur J Heart Fail 2009;11:14–9.
51. Lutolf MP, Hubbell JA. Synthetic biomaterials as instructive extracellular microenvironments for morphogenesis in tissue engineering. Nat Biotechnol 2005;23:47–55.
52. Jawad H, Ali NN, Lyon AR, Chen QZ, Harding SE, Boccaccini AR. Myocardial tissue engineering: a review. J Tissue Eng Regen Med 2007;1:327–42.
53. Uriel S, Labay E, Francis-Sedlak M, et al. Extraction and assembly of tissue-derived gels for cell culture and tissue engineering. Tissue Eng Part C Methods 2009;15:309–21.
54. Badylak SF, Obermiller J, Geddes L, Matheny R. Extracellular matrix for myocardial repair. Heart Surg Forum 2002;6:E20–6.
55. Dorn GW 2nd, Diwan A. The rationale for cardiomyocyte resuscitation in myocardial salvage. J Mol Med 2008;86:1085–95.
56. DeQuach JA, Mezzano V, Miglani A, et al. Simple and high yielding method for preparing tissue specific extracellular matrix coatings for cell culture. PLoS One 2010;5:e13039.
57. Nelson DM, Ma Z, Fujimoto KL, Hashizume R, Wagner WR. Intra-myocardial biomaterial injection therapy in the treatment of heart failure: materials, outcomes and challenges. Acta Biomater 2011;7:1–15.
58. Rane AA, Chuang JS, Shah A, et al. Increased infarct wall thickness by a bio-inert material is insufficient to prevent negative left ventricular remodeling after myocardial infarction. PLoS One 2011;6:e21571.
59. Krishnamurthy P, Rajasingh J, Lambers E, Qin G, Losordo DW, Kishore R. IL-10 inhibits inflammation and attenuates left ventricular remodeling after myocardial infarction via activation of STAT3 and suppression of HuR. Circ Res 2009;104:e9–18.
60. Lin YD, Yeh ML, Yang YJ, et al. Intramyocardial peptide nanofiber injection improves postinfarction ventricular remodeling and efficacy of bone marrow cell therapy in pigs. Circulation 2010;122 Suppl 11:S132–41.
61. Lu WN, Lu SH, Wang HB, et al. Functional improvement of infarcted heart by co-injection of embryonic stem cells with temperature-responsive chitosan hydrogel. Tissue Eng Part A 2009;15:1437–47.
62. Kofidis T, de Bruin JL, Hoyt G, et al. Injectable bioartificial myocardial tissue for large-scale intramural cell transfer and functional recovery of injured heart muscle. J Thorac Cardiovasc Surg 2004;128:571–8.
63. Ifkovits JL, Tous E, Minakawa M, et al. Injectable hydrogel properties influence infarct expansion and extent of postinfarction left ventricular remodeling in an ovine model. Proc Natl Acad Sci U S A 2010;107:11507–12.
64. Silva GV, Perin EC, Dohmann HF, et al. Catheter-based transendocardial delivery of autologous bone-marrow-derived mononuclear cells in patients listed for heart transplantation. Tex Heart Inst J 2004;31:214–9.
65. Lunde K, Solheim S, Aakhus S, et al. Intracoronary injection of mononuclear bone marrow cells in acute myocardial infarction. N Engl J Med 2006;355:1199–209.
66. Laham RJ, Rezaee M, Post M, et al. Intracoronary and intravenous administration of basic fibroblast growth factor: myocardial and tissue distribution. Drug Metab Dispos 1999;27:821–6.
67. Laham RJ, Chronos NA, Pike M, et al. Intracoronary basic fibroblast growth factor (FGF-2) in patients with severe ischemic heart disease: results of a phase I open-label dose escalation study. J Am Coll Cardiol 2000;36:2132–9.
68. Krause K, Jaquet K, Schneider C, et al. Percutaneous intramyocardial stem cell injection in patients with acute myocardial infarction: first-in-man study. Heart 2009;95:1145–52.
69. Chachques JC, Azarine A, Mousseaux E, El Serafi M, Cortes-Morichetti M, Carpentier AF. MRI evaluation of local myocardial treatments: epicardial versus endocardial (Cell-Fix catheter) injections. J Interv Cardiol 2007;20:188–96.

Key Words: biomaterial ▪ extracellular matrix ▪ heart failure ▪ myocardial infarction ▪ scaffold.